Annals of Botany **114**: 325–334, 2014
doi:10.1093/aob/mcu109, available online at www.aob.oxfordjournals.org

ANNALS OF BOTANY
Founded 1887

Modelling the mechanical behaviour of pit membranes in bordered pits with respect to cavitation resistance in angiosperms

Aude Tixier[1,2], Stephane Herbette[1,2], Steven Jansen[3], Marie Capron[4], Philippe Tordjeman[4], Hervé Cochard[1,2] and Eric Badel[1,2,*]

[1]*Clermont Université, Université Blaise Pascal, UMR 547 PIAF, 63000 Clermont-Ferrand, France,* [2]*INRA, UMR 547 PIAF, 63100 Clermont-Ferrand, France,* [3]*Institute for Systematic Botany and Ecology, Ulm University, Albert-Einstein-Allee 11, D-89081 Ulm, Germany and* [4]*Université de Toulouse, INPT-CNRS, Institut de Mécanique des Fluides de Toulouse, Allée du Professeur C. Soula, F-31400 Toulouse, France*
** For correspondence. E-mail eric.badel@clermont.inra.fr*

Received: 14 February 2014 Returned for revision: 2 April 2014 Accepted: 25 April 2014 Published electronically: 10 June 2014

• **Background and Aims** Various correlations have been identified between anatomical features of bordered pits in angiosperm xylem and vulnerability to cavitation, suggesting that the mechanical behaviour of the pits may play a role. Theoretical modelling of the membrane behaviour has been undertaken, but it requires input of parameters at the nanoscale level. However, to date, no experimental data have indicated clearly that pit membranes experience strain at high levels during cavitation events.
• **Methods** Transmission electron microscopy (TEM) was used in order to quantify the pit micromorphology of four tree species that show contrasting differences in vulnerability to cavitation, namely *Sorbus aria*, *Carpinus betulus*, *Fagus sylvatica* and *Populus tremula*. This allowed anatomical characters to be included in a mechanical model that was based on the Kirchhoff–Love thin plate theory. A mechanistic model was developed that included the geometric features of the pits that could be measured, with the purpose of evaluating the pit membrane strain that results from a pressure difference being applied across the membrane. This approach allowed an assessment to be made of the impact of the geometry of a pit on its mechanical behaviour, and provided an estimate of the impact on air-seeding resistance.
• **Key Results** The TEM observations showed evidence of residual strains on the pit membranes, thus demonstrating that this membrane may experience a large degree of strain during cavitation. The mechanical modelling revealed the interspecific variability of the strains experienced by the pit membrane, which varied according to the pit geometry and the pressure experienced. The modelling output combined with the TEM observations suggests that cavitation occurs after the pit membrane has been deflected against the pit border. Interspecific variability of the strains experienced was correlated with vulnerability to cavitation. Assuming that air-seeding occurs at a given pit membrane strain, the pressure predicted by the model to achieve this mechanical state corresponds to experimental values of cavitation sensitivity (P_{50}).
• **Conclusions** The results provide a functional understanding of the importance of pit geometry and pit membrane structure in air-seeding, and thus in vulnerability to cavitation.

Key words: Tree, wood, air-seeding, cavitation resistance, embolism, bordered pit membrane, mechanical modelling, strain, xylem anatomy, *Fagus sylvatica*, beech, *Sorbus aria*, whitebeam, *Populus tremula*, poplar, *Carpinus betulus*, hornbeam.

INTRODUCTION

In angiosperm trees, xylem sap is transported under negative pressure by way of interconnected vessels according to the accepted cohesion–tension theory (Angeles *et al.*, 2004). During drought events, large negative sap pressure increases between vessel ends, and cavitation events could occur. As a result, air could be aspirated from an air-filled vessel to the adjacent functional vessel by way of pores located in the double cell wall: the intervessel pits (Cochard, 2006; Lens *et al.*, 2013). Cavitation may result in an air embolism that leads to a loss of hydraulic conductance (Cochard, 2006). Xylem embolism represents an important constraint on plant survival and productivity (Brodribb and Cochard, 2009; Choat *et al.*, 2012). Thus, xylem functional traits have to manage both water flow efficiency and protection against air entry and propagation in the hydraulic conduit network (Tyree and Zimmermann, 2002).

Intervessel bordered pits are microscopic openings in the double cell wall. They show overarching walls that form a bowl-shaped chamber, which contains in its centre a thin membrane formed from the middle lamella and primary walls (Fig. 1). This airtight membrane is the physical boundary between the two vessels and prevents the spread of air embolisms between vessels. Since the ascent of water between angiosperm vessels involves the crossing of many bordered intervessel pits, the hydraulic behaviour of the pits is a key factor for controlling water movement (Shane *et al.*, 2000; Tyree and Zimmerman, 2002). On the one hand, the flow resistance through intervessel pits accounts for >50 % of the total resistance of the vessel network in angiosperms (Wheeler *et al.*, 2005; Hacke *et al.*, 2006). Their number and their hydraulic

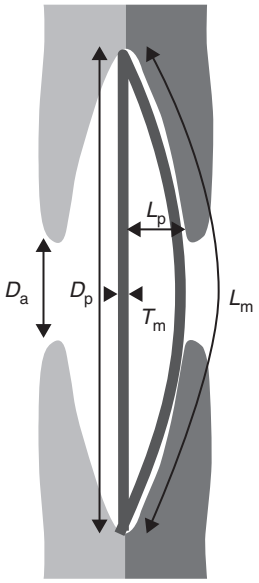

FIG. 1. Diagram of a bordered pit as seen in transverse section. Grey lines show a relaxed and aspirated pit membrane. T_m, pit membrane thickness; L_m, pit membrane length; D_p, pit diameter; L_p, pit chamber depth; D_a, pit aperture diameter.

conductivity, which involves the pit area and its water permeability, are positive factors that improve the intervessel water flow. On the other hand, the pits are the main sites for the air pathway from an air-filled vessel into a functional vessel (Tyree and Sperry, 1989*a*). Altogether, their structure has been reported to reflect a compromise between efficiency and safety of the water flow (Tyree and Sperry, 1989*a*; Choat and Pitterman, 2009; Jansen *et al*., 2009). Cavitation probably occurs in a functional conduit as air bubbles seed from an embolized neighbouring conduit through pores of intervessel pits (Tyree and Zimmermann, 2002; Cochard, 2006). When an embolized vessel is connected by bordered pits to a functional vessel under negative pressure, a pressure difference develops between both sides of the pit membranes. Drought-induced embolism resistance is determined by both qualitative and quantitative pit characteristics (Lens *et al*., 2013; Scholz *et al*., 2013). The probability of air entry into a vessel would increase in a stochastic fashion with its pit area (pit quantity). Considering variability in the porosity of pit membranes, the largest pore of the intervessel pit area will determine air-seeding. The larger the pore, the higher is the chance for the air to spread and to cavitate the vessel (Tyree and Sperry, 1989*b*; Cochard, 2006). The importance of the pit quantity in vulnerability to cavitation has been proposed as the rare pit hypothesis (Jarbeau *et al*., 1995; Wheeler *et al*., 2005; Christman *et al*., 2009). A strong correlation between cavitation resistance and the average area of pit overlap between vessels was found for >80 species (Wheeler *et al*., 2005; Hacke *et al*., 2006; Scholz *et al*., 2013). However, this correlation may not be valid when considering a relatively narrow range of cavitation resistance, suggesting also the importance of qualitative pit features such as pit membrane thickness (Lens *et al*., 2011; Scholz *et al*., 2013).

Recent studies suggested the importance of the structure of pits in xylem functional traits, illustrating interspecific and intraspecific variation of pit membrane porosity (Choat *et al*., 2003, 2008; Sano, 2005; Jansen *et al*., 2009). Pit membrane thickness has been shown to be correlated with pit membrane porosity and thus with the pressure threshold required to force gas across the intervessel pit field (Jansen *et al*., 2009). Intriguingly, the pore size calculated to allow air-seeding was always greater than the pore size measured using perfusion with colloids or scanning electron microscopy (SEM; Choat and Pitterman, 2009; Jansen *et al*., 2009). The discrepancy between observed and calculated pore size can be explained by many factors related to microscope techniques and preparation artefacts. First, microscope methods show limitations for measuring pore sizes in thick membranes (Jansen *et al*., 2009). Secondly, it is difficult to find the largest pore responsible for air-seeding. Thirdly, pits observed under SEM or transmission electron microscopy (TEM) are typically in a relaxed (i.e. non-aspirated) state, whereas pit membrane pores may enlarge by stretching when they undergo a pressure difference across two neighbouring conduits (Tyree and Zimmermann, 2002; Choat *et al*., 2004; Sperry and Hacke, 2004). Silicon injection under pressure allowed the observation of the deflection of pit membranes against the outer pit aperture (Choat *et al*., 2008), illustrating the stretching properties of pit membranes (Thomas, 1972). In such a case, porosity could increase by rupture or reversible stretching of the pit membrane (Sperry and Hacke, 2004). This stretching would then be a function of (1) geometrical characteristics of the membrane and the pit chamber and (2) the intrinsic mechanical properties of the membrane. Experiments based on colloidal gold perfusion across a pit field showed that increasing pressure allowed the perfusion of larger particles through intervessel pit fields (Choat *et al*., 2004). Moreover, since no colloidal gold was found to penetrate pit fields when the pressure was decreased, this study suggested that the increasing pressure difference generated the stretching of the pit membrane.

These recent experimental results strengthen the theoretical hypothesis of Sperry and Hacke (2004) that the mechanical behaviour of the pit structure could be a key point in cavitation resistance. Lens *et al.* (2011) showed a correlation between the pressure required to reduce hydraulic conductance by 50 % (P_{50}) and various pit anatomical features in *Acer* species. Correlations were found for the pit chamber depth, the pit membrane thickness, the pit chamber diameter and the aperture fraction. A mechanistic explanation integrating bordered pit parameters is needed to understand how pit morphological features may control vulnerability to cavitation. The effects of pit geometry on the degree of stretching of the pit membrane have been investigated. Sperry and Hacke (2004) proposed a model of the membrane deflection in response to a pressure difference. They considered the structure of the membrane as a composite material made of the superposition of cellulose microfibril spokes. Starting from this nanoscale level, this very complete modelling was able to evaluate the elastic rigidity of the pit membrane. These data allowed investigation of the theoretical mechanical behaviour of the membrane according to the dimensions of the pit chamber such as its diameter and its depth. Finally, the impact of the membrane deflection on the cavitation process was discussed.

Using a similar mechanical approach to that of Sperry and Hacke (2004), we proposed a mechanical model of the pit membrane under a pressure difference between neighbouring conduits. In our case, the modelling was only based on the geometrical structure of the components of the pit we were able to measure on TEM images, i.e. the chamber depth, the diameter of the membrane and of the aperture, and the thickness of the membrane.

We also obtained proof that pit membranes experience important strains during cavitation events, and our model allowed these strains to be quantified. We investigated the variability of the geometry of the pit structure for several species that show varying cavitation resistance and contrasted bordered pit anatomy in order to test how mechanical properties based on our model may scale with vulnerability to cavitation.

MATERIALS AND METHODS

Plant material

Four species that show a wide range of cavitation sensitivity were used. *Sorbus aria*, *Carpinus betulus*, *Fagus sylvatica* and *Populus tremula* branches were harvested in September 2011 from the Allagnat forest in the centre of France (45°45·23′N, 2°56·26′E, 1000 m a.s.l.). To avoid light effects (Herbette *et al*., 2010), we harvested only fully sun-exposed branches. Samples of 50 cm long were cut from the plants, wrapped in moistened paper and kept at 5 °C in a sealed black plastic bag for a maximum of 6 d. Three samples per species were collected from 1–3 individus. Vulnerability to cavitation measurements and TEM analyses of pits were performed on samples from the same branches.

Vulnerability to cavitation

Xylem vulnerability to cavitation was assessed using the Cavitron (Cochard, 2002; Cochard *et al*., 2005) on 0·28 m long stem samples. The centrifugal force increases water tension in branch segments and allows at the same time measurement of the loss of hydraulic conductance. A vulnerability curve was built by plotting the percentage loss of xylem conductance (PLC) vs. xylem water tension in three branches per species. A sigmoidal function was fitted for each curve using the following equation (Pammenter and Vander Willigen, 1998):

$$\mathrm{PLC} = \frac{100}{1 + e^{[S\,(P - P_{50})/25]}}$$

where P_{50} is the pressure causing 50 % loss of conductance, and S the slope of the curve at this point. In order to investigate the effect of pressure difference on pit membranes, branches of *F. sylvatica* and *P. tremula* were submitted to a −4 MPa pressure with the centrifuge. Then, the central parts of the branches, which correspond to the area with the highest centrifugal forces, were prepared for TEM analysis of pits.

Transmission electron microscopy

Three stem samples of *S. aria*, *C. betulus*, *F. sylvatica* and *P. tremula* were embedded for TEM analysis of pits. Samples were fixed overnight at room temperature using Karnovsky's solution (Karnovsky, 1965). They were then washed in 0·1 m phosphate buffer (pH 7·4) and post-fixed in buffered 1 % osmium tetroxide for 4 h at room temperature. Six washes of 5 min each using phosphate buffer were performed, and samples were gradually dehydrated in ethanol at 4 °C. Samples were embedded in LR white resin (London Resin Company, Reading, UK), which gradually replaced the ethanol. When 100 % LR white resin was reached, the resin was polymerized for 2 d at 55 °C in air-free tubes. Transverse sections with a thickness of 60–90 nm were stained with uranyl acetate for 10 min and lead citrate for 1 min. The TEM observations were carried out using a JEOL JEM1210 transmission electron microscope (JEOL, Tokyo, Japan) at 80 kV accelerating voltage and with a Hitachi H7650 transmission electron microscope. Image analysis was performed using ImageJ software (Schneider *et al*., 2012) with at least 24 intervessel pits studied for each species. Measurements of pit features (Fig. 1, Table 1) were performed on images with pits showing two apertures. We measured pit membrane thickness (T_m), pit chamber depth (L_p), which is defined as the distance from the unaspirated pit membrane to the inner pit aperture, pit chamber diameter (D_p) and pit aperture diameter (D_a). The T_m data were the mean value of three measurements per pit membrane. The L_p and D_a data were the mean values of two measurements per pit. For *P. tremula* and *F. sylvatica*, pit membrane length (L_m) and D_p were measured

TABLE 1. *List of parameters of the pit model with symbols, units, definitions and equations*

Symbol	Unit	Definition	Equation
Constants			
E	Pa	Young's modulus of pit membrane	
ν	–	Poisson's ratio = 0·3	
Input variables			
L_m	µm	Pit membrane length	
D_p	µm	Pit chamber diameter	
L_p	µm	Pit chamber depth, i.e. the distance from the pit membrane surface to the inner pit aperture	
D_a	µm	Pit aperture diameter	
T_m	µm	Pit membrane thickness	
ε_{res}	N	Residual plastic strain	$\varepsilon_{res} = (L_m - D_p)/D_p$
Output variables			
D	MPa µm^{-3}	Pit membrane flexural rigidity	$D = (E \times T_m)/[12\,(1 - \nu^2)]$
ε	–	Maximum pit membrane strain	$\varepsilon_1 = 3 \times (D_p/2) \times (1 - \nu^2)P/(8\,E \times T_m)$ if $P < P_b$ $\varepsilon_2 = 3 \times D_a/2) \times (1 - \nu^2)\,P\,(1 + \varepsilon_1)/(8\,E \times T_m) + \varepsilon_1$ if $P > P_b$
WI_a	µm MPa^{-1}	Pit membrane deflection index	$WI_a = (D_a/2)^4/(64 \times D)$
P_b	MPa	Pressure required to deflect the membrane against the inner aperture	$P_b = (64 \times D \times Lp)/[(D_m/2)^2 - (D_a/2)^2]^2$

and compared between samples submitted to −4 MPa and samples not subject to centrifugal forces. Residual strains (ε_{res}) were calculated as:

$$\varepsilon_{res} = \left(D_p - L_m\right)/D_p$$

Data from the literature

Anatomical and P_{50} data were compiled from previous studies (Sperry and Hacke, 2004; Jansen *et al*., 2009; Plavcová *et al*., 2011; Lens *et al*., 2011; Plavcová and Hacke, 2012). We considered studies for which at least T_m, D_p and P_{50} were measured. Lens *et al.* (2011) compiled T_m, D_p L_p, D_a and P_{50} data for six *Acer* species: *A. negundo*, *A. glabrum* (including var. *glabrum* and var. *diffusum*), *A. grandidentatum*, *A. saccharinum*, *A. platanoides* and*A. pseudoplatanus.* Jansen *et al*., (2009) compiled T_m and D_p data for 12 angiosperm species: *Corylus avellana*, *Fraxinus americana*, *Ilex aquifolium*, *Olea europaea*, *Populus fremontii*, *Quercus robur*, *Salix alba*, *Sambucus nigra*, *Sophora japonica*, *Laurus nobilis*, *Betula nigra* and *Betula pendula*. Corresponding P_{50} values were extracted from Choat *et al.* (2012). D_a measurements were added for *Olea europaea* and *Laurus nobilis*. T_m, D_p, D_a and P_{50} from *Nerium oleander* L. and *Populus trichocarpa* × *deltoides* (clone H11-11) were reported by Sperry and Hacke (2004) and by Plavcová *et al.* (2011) and Plavcová and Hacke (2012), respectively.

Model description

We modelled the mechanical behaviour of the pit membrane in order to quantify (1) the effect of the pressure difference on the strain; (2) the pressure that is required to deflect the membrane against the pit aperture; and (3) the behaviour of the pit membrane beyond the aspiration pressure.

The model assumed circular membranes and was based on the Kirchhoff–Love thin plates theory (Bauchau and Craig, 2009). Basic axioms of this theory consider a continuous, elastic and homogeneous circular plate that (1) can bend in two directions and twist; (2) is initially flat; and (3) shows a transverse dimension (thickness) that is small compared with the diameter. This latter axiom allowed shear effects to be neglected. As a boundary condition, the pit membrane was presumed to be clamped to the pit border. Finally, the pressure was assumed to be uniform on the whole membrane area. All the mechanical parameters were computed for each pit using their intrinsic measured dimensions.

Flexural rigidity (D) of the membrane was calculated as the force couple required to bend the membrane to a unit curvature.

$$D = \frac{(\mathrm{E}\ T_m^3)}{12\ (1-\nu^2)} \tag{1}$$

where E is the Young's modulus of pit membrane and ν is its Poisson's ratio. The Young's modulus is the ratio of stress [σ (Pa)] to strain (ε), and measures the elasticity of a material. Using atomic force microscopy (AFM) on fresh samples, the Young's modulus for intervessel pit membranes in *Populus deltoides* was found to be around 400 MPa (Capron *et al*., 2014). As the available evidence suggests that intervessel pit membranes in angiosperms may show a larger variation in their ultrastructure and chemical composition than previously thought, we used this Young's modulus value by default as a constant value across angiosperm species. Morever, the Poisson coefficient ν, which refers to the transversal contraction of the material, was estimated to be 0·3 for all our computations because most polymers exhibit values of about 0·3. Moreover, this value is in line with the ν value for cellulose (Nakamura *et al*., 2004), which represents the main component of intervessel pit membranes. Considering these elasticity parameters as constants permitted us to focus on how the pit geometry is involved in the interspecific variability of vulnerability to cavitation.

Following the above axioms, the deflection (W) of a membrane that experiences a uniform pressure (P) fulfils the following equation:

$$\nabla^4[W(r)] = \frac{P}{D} \tag{2}$$

In the case of a circular membrane, the Nabla operator (∇) can be written in circular co-ordinates as follows:

$$\frac{\mathrm{d}}{\mathrm{d}r}\left[\frac{1}{r}\frac{\mathrm{d}}{\mathrm{d}r}\left(r\,\frac{\mathrm{d}W(r)}{\mathrm{d}r}\right)\right] = \frac{P}{D} \tag{3}$$

where r is the radial position from the centre of the membrane. Solving this equation using the above-written boundary conditions, leads us to the relationship

$$W(r) = \frac{(R^2 - r^2)^2}{64\ D}\ P \tag{4}$$

where R is the radius of the membrane ($R = D_p/2$). Solving eqn (3) for r being equal to the radius of the aperture ($r = D_a/2$) and W being equal to L_p enabled us to evaluate the pressure required to deflect the pit membrane against the aperture (P_b).

$$P_b = \frac{1}{3}\,\frac{\mathrm{E}}{(1-\nu^2)}\,\frac{T_m^3}{(D_p^2 - D_a^2)^2}\ L_p \tag{5}$$

The strain is the degree of the pit membrane deformation. When P increases, the strain increases as the pit membrane is stretched. According to the mechanical model, the maximum strain level (ε_{max}) occurs at the centre of the pit membrane and increases linearly with P:

$$\varepsilon_{max} = \varepsilon\,(r=0) = -\frac{3}{8}\,\frac{(1-\nu^2)}{\mathrm{E}}\,\frac{R^2}{T_m^2}\ P \tag{6}$$

When $P < P_b$, $R = D_m/2$. However, when $P > P_b$, the peripheral area of the membrane is supported by the pit border and only the membrane region that is not supported by the pit border should be considered for deformation. In this case, assuming that no further displacement occurs at the aperture boundary, we can consider the previous eqns (4) and (6) with $R = D_a/2$.

$\bar{\varepsilon}$ representing the increase in length. In order to calculate $\bar{\varepsilon}$ for a given pressure, it was assumed that the membrane expands to form a spherical arc:

$$\bar{\varepsilon} = \frac{\rho}{R}\ a\sin\left(\frac{R}{\rho}\right) - 1 \tag{7}$$

where ρ is the radius of the sphere in which the deformed membrane is inscribed.

$$\rho = \frac{[R^2 + W(0)^2]}{2\ W(0)} \quad (8)$$

with $R = D_m/2$ if $P < P_b$, and $R = D_a/2$ if $P > P_b$.

Finally, we computed a deflection index (WI_a) on the aperture that was calculated on the basis of eqn (4). This index considered the membrane area that was unsupported by the pit border and was not dependent on pressure. It indicates the ability of the membrane to deflect for a given pressure difference between its two sides.

$$WI_a = \frac{(D_a/2)^4}{64D} \quad (9)$$

The mechanical parameters derived from morphological pit features are reported in Table 1.

RESULTS

Vulnerability to cavitation

Vulnerability to cavitation showed significant differences for P_{50} according to a Student *t*-test. Mean P_{50} values (± s.e.) were −5·67 MPa (±0·17) for *S. aria*, −2·42 MPa (±0·03) for *P. tremula*, −3·18 MPa (±0·16) for *F. sylvatica* and −4·17 MPa (±0·06) for *C. betulus*. PLC values for samples submitted to −4 MPa were 76·7 % (±7·4) and 100 % (±0·0) for *F. sylvatica* and *P. tremula*, respectively.

Quantitative pit characteristics and model inputs

The four species studied showed considerable variation in their pit morphology (Fig. 2A–D; Supplementary Data Table S1). Intervessel pits differed in their pit membrane thickness, but also in diameter, chamber depth and aperture diameter. In addition, differences in pit membrane position and length were observed between pits from control samples of *F. sylvatica* and *P. tremula* (Fig. 2C, D), and pits submitted to a pressure difference of −4 MPa (Fig. 2E, F). The frequency of aspirated pit membranes was clearly higher for −4 MPa samples (2 % for *F. sylvatica* and 17 % for *P. tremula*) compared with the control (0 MPa) samples (0 and 8 % for *F. sylvatica* and *P. tremula*, respectively) (Fig. 2E). Samples of *F. sylvatica* showed a low number of aspirated pit membranes, but deformation of the pit membrane could be seen (Fig. 2F). In addition, the thickness of the pit membrane in aspirated and deformed pit membranes was found to decrease compared with the control conditions. Pit membranes that were aspirated or deformed also showed a higher electron density and were less transparent under TEM than the control samples.

The residual strain ε_{res} (Fig. 3) ranged from 0 to 0·035 for pit membranes of *P. tremula* and from 0 to 0·017 for *F. sylvatica.* The residual strain is a typical pattern that reveals that the membranes experienced large non-recoverable plastic deformation. ε_{res} was significantly different between control samples and −4 MPa samples for both species. *Populus tremula* showed significantly higher ε_{res} than *F. sylvatica*, which is less sensitive to cavitation.

An overview of the pit features for the species studied is shown in Fig. 4. The T_m, D_p, L_p and D_a values varied considerably in

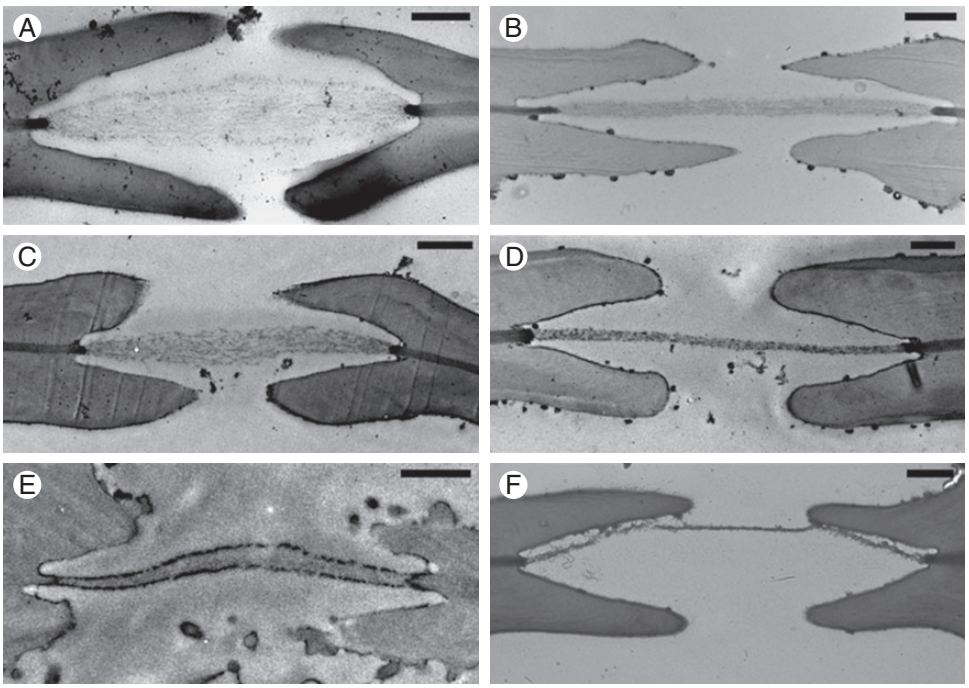

FIG. 2. TEM images of bordered intervessel pits from four species with contrasting vulnerability to cavitation. *Sorbus aria* (A; $P_{50} = -5{\cdot}67 \pm 0{\cdot}17$ MPa, mean ± s.e.), *Carpinus betulus* (B; $P_{50} = -4{\cdot}17 \pm 0{\cdot}06$ MPa), *Fagus sylvatica* (C, E; $P_{50} = -3{\cdot}18 \pm 0{\cdot}16$ MPa) and *Populus tremula* (D, F; $P_{50} = -2{\cdot}42 \pm 0{\cdot}03$ MPa). TEM images are representative pictures of pits observed in control stems (A–D) or stems submitted to a xylem pressure of – 4 MPa (E, F). TEM analysis and vulnerability curves were performed on similar branch samples. Scale bar = 1 μm.

magnitude. Values of D_p for *P. tremula* and *C. betulus* were similar, but were higher than D_p values of *F. sylvatica* and *S. aria*. L_p and D_a showed limited interspecific variability. Nevertheless, *P. tremula* showed pits with significantly deeper chambers (L_p) than other species, and pits of *S. aria* pits had a significantly larger pit aperture diameter (D_a).

There were also differences in intraspecific variability. *Fagus sylvatica* had the highest variability for D_m (Fig. 4B) and D_a (Fig. 4D), while *F. sylvatica* and *S. aria* had high variability for T_m (Fig. 4A).

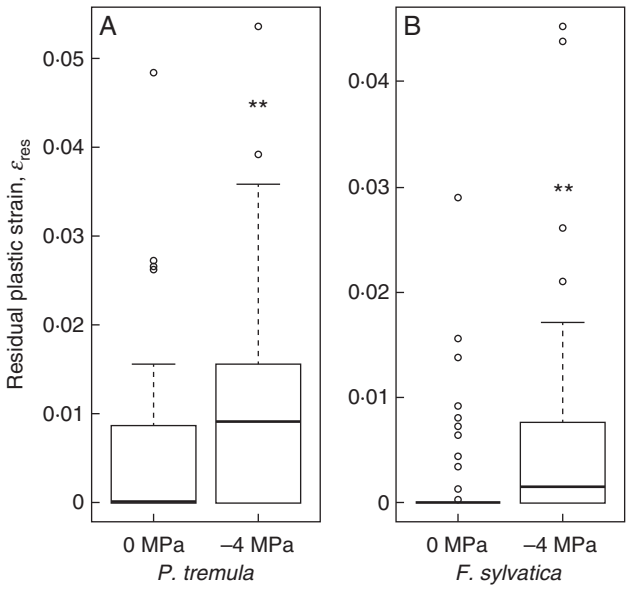

FIG. 3. Residual strain in pit membranes induced during cavitation events in *Populus tremula* (A) and *Fagus sylvatica* (B). Stem samples were control stems (0 MPa) or stems subject to – 4 MPa. Pit membrane length (L_m) was compared with pit chamber diameter (D_p) and the residual plastic strain was calculated as $\varepsilon_{res} = (L_m - D_p)/D_p$. Significant differences ($P < 0{\cdot}01$, Wilcoxon rank sum test) are shown by asterisks.

Mechanical characteristics of the pit structure and model outputs

Figure 5 shows the relationship between the mechanical properties of the pits (D and WI_a) and P_{50}. The pit membrane flexural rigidity (D) was calculated for each pit based on its membrane thickness T_m for 25 angiosperm species including the four species studied. D showed an exponential relationship with P_{50} ($R^2 = 0{\cdot}72$). Species showing higher cavitation resistance had higher D. The pit membrane deflection index (WI_a) was calculated using T_m and D_a for 14 angiosperm species and showed a strong relationship with P_{50} ($R^2 = 0{\cdot}86$). Species showing higher cavitation resistance had a lower deflection index.

The measurements of D_m, D_a, T_m and L_p for *S. aria*, *C. betulus*, *F. sylvatica* and *P. tremula* (Fig. 4) allowed modelling the maximum (ε_{max}) and mean ($\bar{\varepsilon}$) pit membrane strain as a function of pressure (P; Fig. 6). The maximum strain (Fig. 6A) occurs at the centre of the membrane, whereas the mean strain (Fig. 6B) represents the increase in the total membrane length. When the pit membrane reaches the aperture and is fully aspirated at the P_b pressure, there is a breakpoint in the strain function. Beyond this P_b value, only the pit membrane area that is not supported by the borders is deformed. The membrane strains ranged from 0 to 0·15. A different behaviour of pit membrane strain was observed for a low pressure. When P was >2 MPa, species with higher vulnerability to cavitation tended to experience higher levels of strain. When P exceeded P_b, the slope of the strain was higher for ε than for $\bar{\varepsilon}$.

The relationship between the mechanical properties based on our model and the vulnerability to cavitation was tested in 11 angiosperm species (Fig. 7). P_b and P_{50} (Fig. 7A) were strongly correlated ($R^2 = 0{\cdot}73$). In general, P_b was <1 MPa, and less negative than the P_{50} value for all species studied, except for *S. aria*.

DISCUSSION

Our observations that show residual strains provide experimental proof that the pit membrane may undergo strains during air-seeding events. This corroborates recent results of Capron

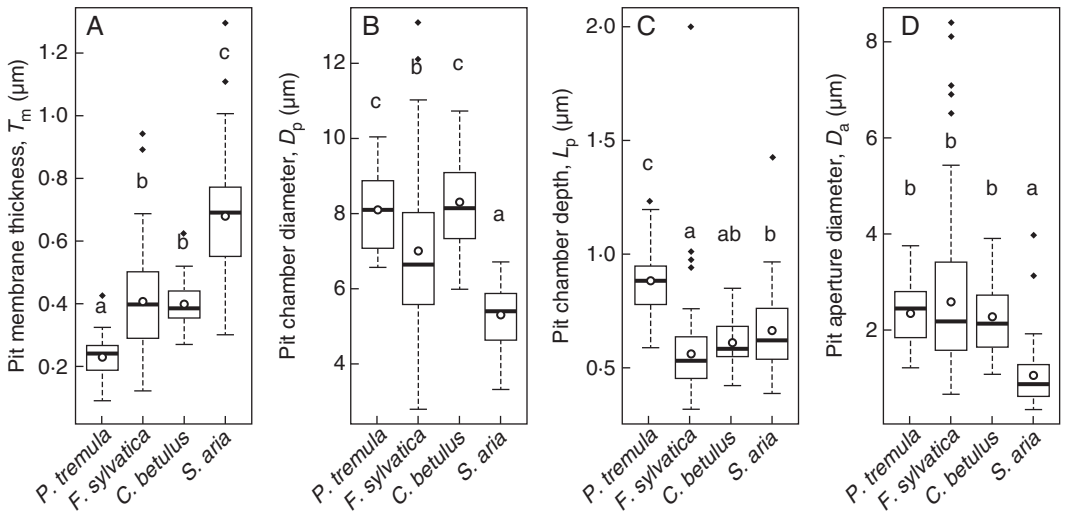

FIG. 4. Comparison of pit anatomical features measured in four species with contrasting vulnerability to cavitation. Three stem samples were prepared for TEM. Pit membrane thickness (T_m), pit diameter (D_m), pit chamber depth (L_p) and pit aperture diameter (D_a) were measured under TEM for 24–69 pits per species. Red dots represent mean values and letters indicate significant differences between groups ($P < 0{\cdot}05$, ANOVA, Tukey). The species order from left to right is according to increasing cavitation resistance.

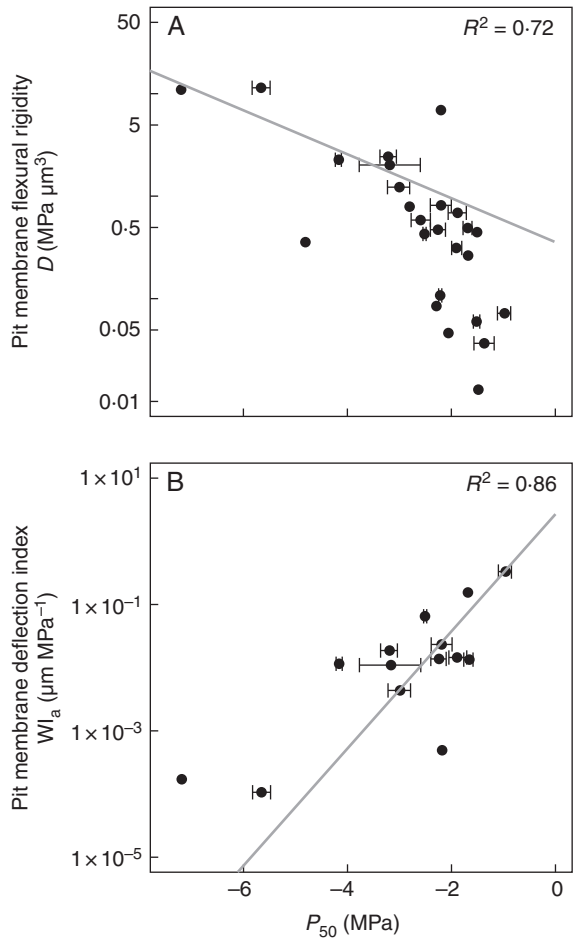

FIG. 5. Relationships between mechanical properties of the pit membrane (D, WI_a) and P_{50}. Pit membrane flexural rigidity (D) was calculated based on the pit membrane thickness (T_m) for 25 angiosperms species (A). The pit membrane deflection index (WI_a) was calculated using mean pit values of T_m and D_a for 14 angiosperms species (B). Data are means values (± s.e.). The y-axis is log scaled. Exponential regression lines are indicated in grey.

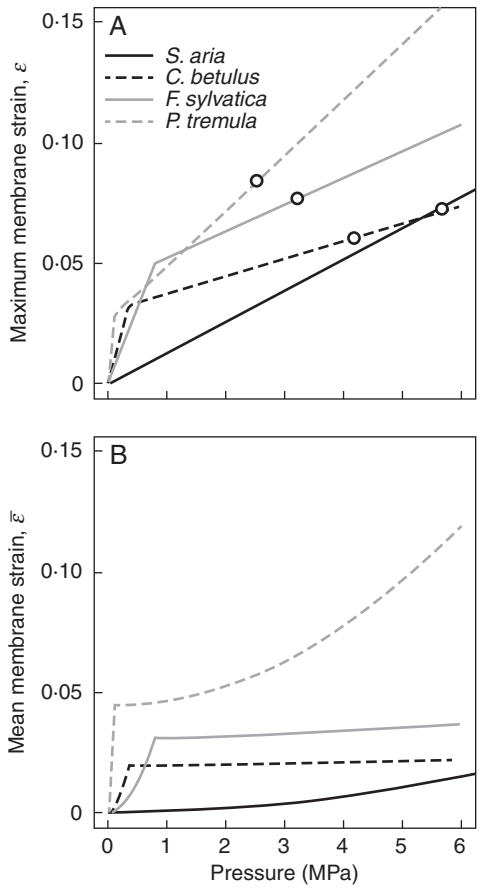

FIG. 6. Maximum pit membrane strain (ε_{max}) vs. pressure in four species with constrasting vulnerability to cavitation. Mean values of pit features were used to calculate pit membrane maximum (ε) and mean ($\bar{\varepsilon}$) strain in *S. aria*, *C. betulus*, *F. sylvatica* and *P. tremula* (as indicated in the key). The maximum strain occurs at the centre of the membrane, whereas the mean strain represents the relative increase in membrane length. Strains increase as the pit membrane is aspirated against the pit border. When the pit membrane reaches the pit border for a given pressure P_b, there is a breakpoint in the strain function. The P_b pressure differs between the species and can be deduced from the change in the slope of the strain function. Beyond this P_b value, only the pit membrane area that is unsupported by the aperture is deformed. The circles in (A) indicate the P_{50} values.

et al. (2014) who measured the deflection of membranes after silicon injection for different pressures. We propose a model of a pit membrane that undergoes a pressure difference between neighbouring conduits. This integrative model considers various morphological features of the bordered pit. The mechanical output of the model showed that variability of the pit features leads to a great interspecific variability of the pit membrane strains for a given pressure. These strains were correlated with P_{50} among the species studied and permitted us to present a functional understanding of the importance of the pit geometry for vulnerability to cavitation.

Modelling the pit membrane behaviour under pressure

Mechanical behaviour of the pit membrane in response to pressure is a function of its structure, which is determined by geometrical parameters (Fig. 1) and the intrinsic mechanical properties of the pit membrane. The pit membrane elasticity (E) or its Poisson's coefficient (ν) depends on the composition and microstructure of the membrane (Sperry *et al.*, 2004; Herbette and Cochard, 2010; Lens *et al.*, 2013). So far, interspecific variability of E has not been investigated because of the technical difficulty in applying AFM measurements on wet (i.e. fresh) pit membranes (Pesacreta *et al.*, 2005; Zwieniecki and Secchi, 2012). We used the only available value (Capron *et al.*, 2014). If E should depend on the thickness of the membrane because of the number of cellulose microfibrils sheets (Sperry and Hacke, 2004), it should also be influenced by the composition of the membrane and the cross-links between components. Equations (5) and (6) show that the pressure required for the membrane to reach the pit border (P_b) varies linearly with E, and the membrane deformation is inversely proportional to E. Considering ν and E as constant parameters permitted us to focus on the role of the pit geometry and the involvement of simple and measurable anatomical parameters in the interspecific variability to cavitation resistance. Moreover, we should consider the point that we modelled the aspirated pit membrane as a clamped circular plate that does not slip against the pit border.

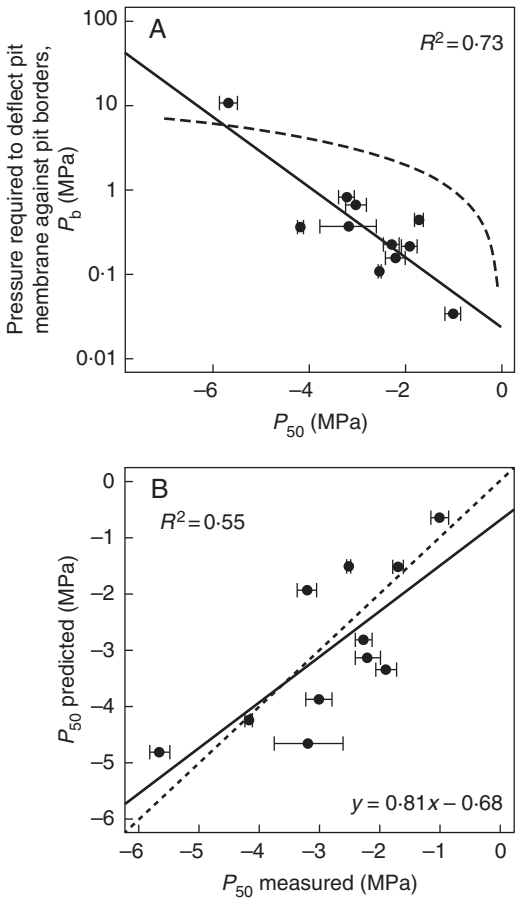

FIG. 7. (A) Relationships between mechanical properties of bordered intervessel pits and cavitation sensitivity (P_{50}). The relationship was tested for *S. aria*, *C. betulus*, *F. sylvatica*, *P. tremula* and six *Acer* species. P_b was deduced from bordered pit features and plotted against P_{50} values measured experimentally. Note the log scale on the *y*-axis. (B) Assuming the air-seeding occurs for a given maximum membrane strain ($\varepsilon = 0{\cdot}06$), the model allowed us to evaluate the corresponding P_{50} pressure which is compared with experimental P_{50} values. Data are means values (± s.e.). Exponential regression lines are solid, and the dotted line represents the $P_b = P_{50}$ line.

The statistical distribution of the geometrical features was variable and depended on the species. Moreover, TEM observations do not ensure that the thin transverse sections we observed were all exactly in the centre of the pit. This does not affect the membrane thickness measurements but probably leads to an underestimation of the pit diameter, pit depth and aperture diameter. However, measuring the pit dimensions close to the aperture probably ensured that measurements were performed close to the optimal position. This also suggests that the measurements of a large number of pits are required in order to evaluate the mean character of a species. Pits differed in their pit membrane thickness, which is correlated with the pore size (Jansen *et al.*, 2009). We show that the pit membrane thickness can also be a trait influencing the mechanical behaviour of the pit membrane. The effects of the pit membrane thickness on its porosity and mechanical behaviour could be complementary and explain the strong correlation of this anatomical feature with P_{50}. The species studied also showed variation in terms of pit diameter, pit chamber depth and pit aperture diameter. While *F. sylvatica* and *C. betulus*, for instance, show similar membrane thickness (T_m) values, T_m on its own does not explain the clear difference in vulnerability to cavitation between both species. T_m, D_a, D_p and L_p differed among the species studied in relation to their vulnerability to cavitation. Despite good results obtained with our mechanical model, some limitations should also be considered regarding the use of mean values, as the variability in pit morphology cannot be neglected. Another shortcoming of our model is that it is based on circular pit membranes. However, an elliptical pit shape is common, and considerable variation among the species studied was found for the pit aperture diameter (D_a) and for the pit diameter (D_p) in *F. sylvatica*. Our results also illustrate that it is important to compute the mechanical parameters using the full range of morphological variation of pit characters and not to compute mechanical parameters using mean values. While TEM images do not allow measurement of the pit circularity, SEM observations showing the surface view of bordered pits would be required to quantify circularity.

Relationship between pit geometry and vulnerability to cavitation

Although *F. sylvatica* and *C. betulus* had similar values for membrane thickness, they had different pit chamber geometry, in particular the pit diameter (D_p). Modelling of the pit behaviour showed that high pressure generated contrasted interspecific strains that could explain their great difference in vulnerability to cavitation. The relationship found by Lens *et al.* (2011) between the chamber depth (L_p) and P_{50} was not observed in the four species we studied. In order to understand the involvement of the pit geometry in vulnerability to cavitation, the anatomical features of the pit were integrated into the ε values.

The residual strains in pit membranes after cavitation events in *P. tremula* and *F. sylvatica* (Fig. 3) supported the relevance of the modelling of pit membrane strains. The least cavitation-resistant species showed the highest residual strains. This observation also suggested that the cavitation process may be linked to large non-recoverable plastic strains that occur when high pressures are experienced (Choat *et al.*, 2004) and that could also explain the cavitation fatigue phenomenon.

In order to investigate a relationship between pit geometry and vulnerability to cavitation, parameters derived from the model were computed and plotted against P_{50} (Fig. 5). First the membrane rigidity D showed a stronger correlation with P_{50} ($R^2 = 0{\cdot}72$) than the membrane thickness T_m alone ($R^2 = 0{\cdot}66$). Moreover, the pit membrane rigidity adds an important mechanical role to T_m with respect to cavitation resistance. The deflection index (WI_a) appears to be a relevant parameter to investigate pit membrane behaviour. WI_a integrates the size of the pit aperture D_a, which appears to be an important feature of the pit geometry, and affects the behaviour of an aspirated pit membrane. In general, the pit aperture D_a represents a rather small and constant fraction of the pit border D_p, with a pit aperture of around 10 % of the pit membrane area (Lens *et al.*, 2011; Scholz *et al.*, 2013). According to our modelling, the pressure required to deflect the pit membrane against its aperture is low (<1 MPa). This corroborates the results obtained by the modelling of Sperry and Hacke (2004) who concluded that aspiration should probably occur early before air-seeding. Also, most of the strain occurs in the aperture. The high correlation between P_{50} and the deflection index WI_a ($R^2 = 0{\cdot}86$) argues that this parameter could be a key point for cavitation resistance.

Strains experienced by the membrane represent a suitable parameter to investigate the functional link between mechanical behaviour and resistance to cavitation. On the one hand, the strains experienced by the membrane may affect air-seeding via enlarging pores (Choat *et al.*, 2003, 2004; Choat and Pittermann, 2009). On the other hand, the pit membrane may encounter some permanent damage, which could also lead to air-seeding (Sperry and Hacke, 2004). The computation of the strains showed contrasting results between the four species (Fig. 6). The pit membranes of *P. tremula*, which was the most vulnerable species, were rapidly deflected against the aperture for a pressure P_b value of 0·11 MPa and then underwent the highest strains in the aperture. A thin membrane with a large diameter explained this behaviour. Similarly, the pit membranes of *C. betulus* were rapidly deflected against the aperture for a P_b of 0·35 MPa because of a large membrane area, but the strains increased slowly because of a small aperture diameter that made the structure more rigid. The pit membranes of *F. sylvatica* were aspirated for a higher P_b than for *C. betulus* because of small pit membrane diameters. However, compared with *C. betulus*, pits of *F. sylvatica* had a larger aperture D_a, which resulted in a higher slope of the strain vs. pressure (P) function when P exceeded P_b. The lower vulnerability to cavitation for *C. betulus* can thus be attributed to the pit geometry that limits the membrane deformation rather than the intrinsic property of its pit membrane. Finally, the pit structure of *S. aria* required a much higher P_b (10·76 MPa) than the pit membranes of more vulnerable species. A thick membrane bearing a small diameter explained the high value for P_b. The strains experienced by pit membranes in this species at 5 MPa were much lower than those of the three more vulnerable species. It is noteworthy that the strains experienced at high pressure difference were in accordance with the vulnerability to cavitation of the four species. However, considering the T_m/D_p ratio of pit membranes in *S. aria* ($T_m/D_p = 0{\cdot}12 \pm 0{\cdot}007$), the use of the thin plate theory remains questionable. This theory does not involve shear deformations and should only be applicable for pit membranes having a thickness to pit diameter ratio of $<0{\cdot}05$ (Zietlow *et al.*, 2012). Thus the computations for *S. aria* are likely to underestimate the strains and deflection. This reservation could be applicable to other species, and the thick plate theory would be more relevant to model their membrane behaviour.

Figure 7 shows the involvement of the pit geometry in interspecific variability of vulnerability to cavitation. If the pressure required to deflect the pit membrane against its aperture (P_b) has no direct mechanistic involvement in air-seeding, its relationship to P_{50} is interesting because the P_b parameter (1) integrates all pit features, including membrane, chamber and aperture dimensions; (2) has a strong impact on the strain experienced by the membrane; and (3) reveals different pit strategies among species. A strong correlation with P_{50} was found, and P_b always seemed to be lower than P_{50}, except for *S. aria*, confirming the importance of the strains experienced by the membrane when it is deflected against the pit border. Comparison of computed P_b values and P_{50} values suggested that the air-seeding events occur when the pit membrane has already been deflected against the pit border (Fig. 6A).

Moreover, we computed the maximum pit membrane strain for $P = P_{50}$ and we observed a low variability. Thus, assuming the P_{50} values correspond to a constant critical pit membrane strain ($\varepsilon = 0{\cdot}06$), the model allowed evaluation of the corresponding pressure that is required to reach this mechanical state [eqn (6)]. This predicted value was then compared with experimental values for a set of 11 species (Fig. 7B). The correlation found suggests that the structure of the pit has a large impact on the cavitation resistance and that the air-seeding occurs when the pit membrane strain exceeds a threshold value that probably corresponds to mechanical damage.

Broadening our model to a larger number of species would provide insight into various evolutionary strategies of angiosperm pit membranes. According to our model, decreasing the diameter of the pit D_p showed the largest effect on the strains compared with other features of the pit. However, the correlation between pit diameter only and cavitation resistance tends to be low (Lens *et al.*, 2011; Scholz *et al.*, 2013). This corroborates the idea that not a single feature but rather various dimensions of the bordered pit can be adjusted and influence cavitation resistance. The gain in decreasing vulnerability to cavitation could be at the cost of a less efficient water flow in the pit chamber. This 'trade-off' hypothesis has been investigated by Sperry and Hacke (2004) who modelled the pit hydraulic efficiency in relation to the geometry of the bordered pits. However, their investigations finally showed no relationship between pit flow resistance and resistance to cavitation. Moreover, sensitivity analysis and covariance analysis of pit features would be of interest on a broader data set of species.

Insights into the mechanism of cavitation

The putative role of the deflection of the pit membrane has been investigated previously (Sperry and Hacke, 2004; Choat *et al.*, 2008). Here, residual strains in pit membranes induced during cavitation events in *P. tremula* and *F. sylvatica* (Fig. 3) provided experimental proof that the pit membrane undergoes mechanical strains during cavitation. The advantage of TEM observations is that residual strains were quantified and compared between species.

Calculation of strains provides insights into the mechanisms of cavitation through air-seeding. First, the low pressure P_b calculated in this study corroborates the hypothesis that air-seeding should occur when the membrane is aspirated against the aperture. Thus, air-seeding probably occurs in the central region of the membrane that is not supported by the pit borders and subjected to the maximum strain. The strains experienced on the whole membrane inside the chamber alone cannot explain interspecific variability, because strains occur at low pressures that do not correspond to air-seeding pressure. The strains estimated by our model (Fig. 6) appear realistic, because they were higher than the residual plastic strains (Fig. 3). The membrane deformations would range from 5 to 15 % for such high pressures. The resulting enlargement of pores in pit membranes or their formation of micro cracks could be involved in air-seeding. Pore diameters calculated from the Laplace law are always larger than maximum pore diameters measured from SEM images (Jansen *et al.*, 2009). Pit membrane strains would increase the pore diameter and could partially explain this difference. Considering the low range of deformation the membrane could experience, and according to the Laplace law, a 10 % increase in the pore diameter would be negligible for air-seeding pressure and too weak to explain the discrepancy between the observed and expected pore size (Jansen *et al.*, 2009). Thus, our results reinforce the

hypothesis that air-seeding is probably not due to pit membrane pore enlargement. Alternatively, the residual plastic strains observed suggest that the pit membrane may experience some structural damage when air-seeding occurs. The observation of cavitation fatigue also supports the pit membrane rupture hypothesis (Hacke *et al*., 2001). The comparison between ε and $\bar{\varepsilon}$ opens the discussion on the point where the membrane air-seeding occurs. If pores have a more or less similar diameter across the pit membrane area, which would be expected based on the equal thickness of angiosperm pit membranes, then air-seeding should occur mostly in the middle of the membrane where maximum strain is experienced. SEM analyses of pits tend to support this hypothesis (Choat *et al*., 2004). In contrast, if we consider some variability in pore diameter and the idea that the largest pore is randomly distributed on the pit membrane surface (Sano, 2005), the mean membrane strain should be considered as a relevant parameter to evaluate air-seeding resistance. Both hypotheses are relevant and the debate will continue until the mechanisms of air-seeding are understood.

SUPPLEMENTARY DATA

Supplementary data are available online at www.aob.oxfordjournals.org and consist of Table S1: interspecific variability of the pit structure, with measurements performed using TEM images.

ACKNOWLEDGEMENTS

The authors thank the electron microscopy section of Ulm University for assistance with TEM. This research was founded in part by the PitBulles project (ANR no. 2010 Blanc 171001).

LITERATURE CITED

Angeles G, Bond B, Boyer JS, *et al*. 2004. The cohesion–tension theory. *New Phytologist* **163**: 451–452.

Bauchau A, Craig JI. 2009. Kirchhoff plate theory. In: *Structural analysis*. Berlin: Springer, 819–914.

Brodribb TJ, Cochard H. 2009. Hydraulic failure defines the recovery and point of death in water-stressed conifers. *Plant Physiology* **149**: 575–584.

Capron M, Charru F, Badel E, Cochard H, Tordjeman P. 2014. Gas flow in plant microfluidic networks controlled by capillary valves. *PhysRevE* doi: 10.1103/PhysRevE.89.033019.

Choat B, Pittermann J. 2009. New insights into bordered pit structure and cavitation resistance in angiosperms and conifers. *New Phytologist* **182**: 557–560.

Choat B, Ball M, Luly J, Holtum J. 2003. Pit membrane porosity and water stress-induced cavitation in four co-existing dry rainforest tree species. *Plant Physiology* **131**: 41–48.

Choat B, Jansen S, Zwieniecki MA, Smets E, Holbrook NM. 2004. Changes in pit membrane porosity due to deflection and stretching: the role of vestured pits. *Journal of Experimental Botany* **55**: 1569–1575.

Choat B, Cobb AR, Jansen S. 2008. Structure and function of bordered pits: new discoveries and impacts on whole-plant hydraulic function. *New Phytologist* **177**: 608–625.

Choat B, Jansen S, Brodribb TJ, *et al*. 2012. Global convergence in the vulnerability of forests to drought. *Nature* **491**: 752–755.

Christman M, Sperry JS, Adler FR. 2009. Testing the 'rare pit' hypothesis for xylem cavitation resistance in three species of Acer. *New Phytologist* **182**: 664–674.

Cochard H. 2002. A technique for measuring xylem hydraulic conductance under high negative pressures. *Plant, Cell and Environment* **25**: 815–819.

Cochard H. 2006. Cavitation in trees. *Comptes Rendus Physique* **7**: 1018–1026.

Cochard H, Damour G, Bodet C, Tharwat I, Poirier M, Améglio T. 2005. Evaluation of a new centrifuge technique for rapid generation of xylem vulnerability curves. *Physiologia Plantarum* **124**: 410–418.

Hacke UG, Stiller V, Sperry JS, Pittermann J, McCulloh K. 2001. Cavitation fatigue. Embolism and refilling cycles can weaken the cavitation resistance of xylem. *Plant Physiology* **125**: 779–786.

Hacke UG, Sperry JS, Wheeler JK, Castro L. 2006. Scaling of angiosperm xylem structure with safety and efficiency. *Tree Physiology* **26**: 689–701.

Herbette S, Cochard H. 2010. Calcium is a major determinant of xylem vulnerability to cavitation. *Plant Physiology* **153**: 1932–1939.

Herbette S, Wortemann R, Awad H, Huc R, Cochard H, Barigah TS. 2010. Insights into xylem vulnerability to cavitation in Fagus sylvatica L.: phenotypic and environmental sources of variability. *Tree Physiology* **30**: 1448–1455.

Jansen S, Choat B, Pletsers A. 2009. Morphological variation of intervessel pit membranes and implications to xylem function in angiosperms. *American Journal of Botany* **96**: 409–419.

Jarbeau JA, Ewers FW, Davis SD. 1995. The mechanism of water-stress-induced embolism in two species of chaparral shrubs. *Plant, Cell and Environment* **18**: 189–196.

Karnovsky M. 1965. A formaldehyde–glutaraldehyde fixative of high osmolality for use in electron microscopy. *Journal of Cell Biology* **27**: 137–138.

Lens F, Sperry John S, Christman M, Choat B, Rabaey D, Jansen S. 2011. Testing hypotheses that link wood anatomy to cavitation resistance and hydraulic conductivity in the genus Acer. *New Phytologist* **190**: 709–723.

Lens F, Tixier A, Cochard H, Sperry JS, Jansen S, Herbette S. 2013. Embolism resistance as a key mechanism to understand adaptive plant strategies. *Current Opinion in Plant Biology* **16**: 297–292.

Nakamura K, Wada M, Kuga S, Okano T. 2004. Poisson's ratio of cellulose I and cellulose II. *Journal of Polymer Science Part B: Polymer Physics* **42**: 1206–1211.

Pammenter NW, Vander Willigen C. 1998. A mathematical and statistical analysis of the curves illustrating vulnerability of xylem to cavitation. *Tree Physiology* **18**: 589–593.

Pesacreta TC, Groom LH, Rials TG. 2005. Atomic force microscopy of the intervessel pit membrane in the stem of *Sapium sebiferum* (Euphorbiaceae). *International Association of Wood Anatomists Journal* **26**: 397–426.

Plavcová L, Hacke UG. 2012. Phenotypic and developmental plasticity of xylem in hybrid poplar saplings subjected to experimental drought, nitrogen fertilization, and shading. *Journal of Experimental Botany* **63**: 695–709.

Plavcová L, Hacke UG, Sperry JS. 2011. Linking irradiance-induced changes in pit membrane ultrastructure with xylem vulnerability to cavitation. *Plant, Cell and Environment* **34**: 501–513.

Sano Y. 2005. Inter and intraspecific structural variations among intervascular pit membranes as revealed by field-emission scanning electron microscopy. *American Journal of Botany* **92**: 1077–1084.

Schneider C., Rasband WS, Eliceiri K. 2012. NIH Image to ImageJ: 25 years of image analysis. *Nature Methods* **9**: 671–675.

Scholz A, Rabaey D, Stein A, Cochard H, Smets E, Jansen S. 2013. The evolution and function of vessel and pit characters with respect to cavitation resistance across 10 *Prunus* species. *Tree Physiology* **33**: 684–694.

Shane M, Cully M, Canny M. 2000. Architecture of branch–root junctions in maize: structure of the connecting xylem and the porosity of pit membranes. *Annals of Botany* **85**: 613–624.

Sperry JS, Hacke UG. 2004. Analysis of circular bordered pit function. Angiosperm vessels with homogenous pit membranes. *American Journal of Botany* **91**: 369–385.

Thomas RJ. 1972. Bordered pit aspiration in angiosperms. *Wood and Fiber* **3**: 236–237.

Tyree MT, Sperry JS. 1989*a*. Vulnerability of xylem to cavitation and embolism. *Annual Review of Plant Physiology and Molecular Biology* **40**: 19–38.

Tyree MT, Sperry JS. 1989*b*. Characterization and propagation of acoustic emission signals in woody plants: towards an improved acoustic emission counter. *Plant, Cell and Environment* **12**: 371–382.

Tyree MT, Zimmermann MH. 2002. *Xylem structure and the ascent of sap*, 2nd edn. Berlin: Springer.

Wheeler JK, Sperry JS, Hacke Uwe G, Hoang N. 2005. Inter-vessel pitting and cavitation in woody Rosaceae and other vesselled plants: a basis for a safety versus efficiency trade-off in xylem transport. *Plant, Cell and Environment* **28**: 800–812.

Zietlow DW, Griffin DC, Moore TR. 2012. The limitations on applying classical thin plate theory to thin annular plates clamped on the inner boundary. *AIP Advances* **2**: 042103-1–042103-8.

Zwieniecki MA, Secchi F. 2012. Getting variable xylem hydraulic resistance under control: interplay of structure and function. *Tree Physiology* **32**: 1431–1433.